THE APPLICATION OF MULTIWAVELET FILTER BANKS TO IMAGE PROCESSING*

V. Strela[†,‡], P. N. Heller[‡], G. Strang[†], P. Topiwala[§], C. Heil[¶,§]

Abstract

Multiwavelets are a new addition to the body of wavelet theory. Realizable as matrix-valued filter banks leading to wavelet bases, multiwavelets offer simultaneous orthogonality, symmetry, and short support, which is not possible with scalar 2-channel wavelet systems. After reviewing this recently developed theory, we examine the use of multiwavelets in a filter bank setting for discrete-time signal and image processing. Multiwavelets differ from scalar wavelet systems in requiring two or more input streams to the multiwavelet filter bank. We describe two methods (repeated row and approximation/deapproximation) for obtaining such a vector input stream from a one-dimensional signal. Algorithms for symmetric extension of signals at boundaries are then developed, and naturally integrated with approximation-based preprocessing. We describe an additional algorithm for multiwavelet processing of two-dimensional signals, two rows at a time, and develop a new family of multiwavelets (the constrained pairs) that is well-suited to this approach. This suite of novel techniques is then applied to two basic signal processing problems, denoising via wavelet-shrinkage, and data compression. After developing the approach via model problems in one dimension, we applied multiwavelet processing to images, frequently obtaining performance superior to the comparable scalar wavelet transform.

EDICS category: IP 1.6

submitted to *IEEE Trans. on Image Processing*

Contact address:
Peter Niels Heller
Aware, Inc.
One Oak Park
Bedford, MA 01730-1413
Phone: (617) 276-4000
FAX: (617) 276-4001
email: heller@aware.com

*Work at Aware, Inc. was supported in part by the Advanced Research Projects Agency of the Department of Defense and monitored by the Air Force Office of Scientific Research under contract no. F49620-92-C-0054. Work at the MITRE Corporation was sponsored by the MITRE Sponsored Research Project.

[†]Massachusetts Institute of Technology, Cambridge, MA 02139

[‡]Aware Inc., Bedford, MA 01730

[§]MITRE Corp., Bedford, MA 01730

[¶]Georgia Institute of Technology, Atlanta, GA 30332

1 Introduction

Wavelets are a useful tool for signal processing applications such as image compression and denoising. Until recently, only *scalar* wavelets were known: wavelets generated by *one* scaling function. But one can imagine a situation when there is *more than one* scaling function [12]. This leads to the notion of *multiwavelets*, which have several advantages in comparison to scalar wavelets [26]. Such features as short support, orthogonality, symmetry, and vanishing moments are known to be important in signal processing. A scalar wavelet *cannot* possess all these properties at the same time [25]. On the other hand, a multiwavelet system *can* simultaneously provide perfect reconstruction while preserving length (orthogonality), good performance at the boundaries (via linear-phase symmetry), and a high order of approximation (vanishing moments). Thus multiwavelets offer the possibility of superior performance for image processing applications, compared with scalar wavelets.

We describe here novel techniques for multirate signal processing implementations of multiwavelets, and present experimental results for the application of multiwavelets to signal denoising and image compression. The paper is organized as follows. Section 2 reviews the definition and construction of continuous-time multiwavelet systems, and Section 3 describes the connection between multiwavelets and matrix-valued multirate filterbanks. In Section 4 we develop several techniques for applying multiwavelet filter banks to one-dimensional signals, including approximation-based preprocessing and symmetric extension for finite-length signals. Two-dimensional signal processing offers a new set of problems and possibilities for the use of multiwavelets; we discuss several methods for the two-dimensional setting in Section 5, including a new family of multiwavelets, the constrained pairs. Finally, in Section 6 we describe the results of our application of multiwavelets to signal denoising and data compression.

2 Multiwavelets — several wavelets with several scaling functions

As in the scalar wavelet case, the theory of multiwavelets is based on the idea of multiresolution analysis (MRA). The difference is that multiwavelets have several scaling functions. The standard multiresolution has one scaling function $\phi(t)$:

- The translates $\phi(t-k)$ are linearly independent and produce a basis of the subspace V_0;
- The dilates $\phi(2^j t - k)$ generate subspaces V_j, $j \in \mathbf{Z}$, such that

$$\cdots \subset V_{-1} \subset V_0 \subset V_1 \subset \cdots \subset V_j \subset \cdots$$

$$\overline{\bigcup_{j=-\infty}^{\infty} V_j} = L^2(\mathbf{R}), \qquad \bigcap_{j=-\infty}^{\infty} V_j = \{0\}\,.$$

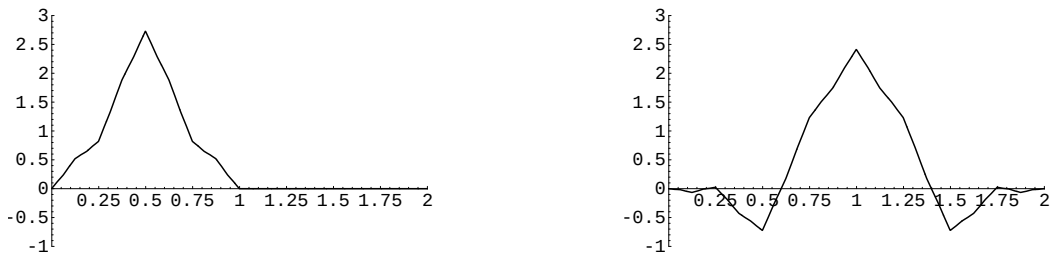

Figure 1: Geronimo–Hardin–Massopust pair of scaling functions.

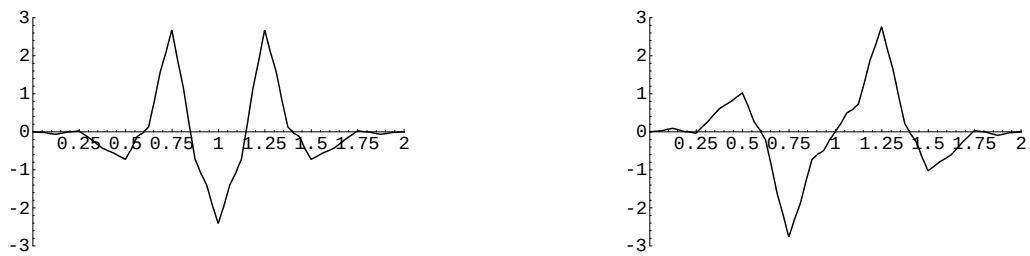

Figure 2: Geronimo–Hardin–Massopust multiwavelets.

- There is one wavelet $w(t)$. Its translates $w(t-k)$ produce a basis of the "detail" subspace W_0 to give V_1:

$$V_1 = V_0 \oplus W_0.$$

For multiwavelets, the notion of MRA is the same except that now a basis for V_0 is generated by translates of N scaling functions $\phi_1(t-k)$, $\phi_2(t-k)$, $\ldots, \phi_N(t-k)$. The vector $\Phi(t) = [\phi_1(t), \ldots, \phi_N(t)]^T$, will satisfy a *matrix* dilation equation (analogous to the scalar case)

$$\Phi(t) = \sum_k C[k]\Phi(2t-k). \tag{1}$$

The coefficients $C[k]$ are N by N matrices instead of scalars.

Associated with these scaling functions are N wavelets $w_1(t), \ldots, w_N(t)$, satisfying the *matrix* wavelet equation

$$W(t) = \sum_k D[k]\Phi(2t-k). \tag{2}$$

Again, $W(t) = [w_1(t), \ldots, w_N(t)]^T$ is a vector and the $D[k]$ are N by N matrices.

As in the scalar case, one can find the conditions of orthogonality and approximation for multiwavelets [26, 27, 14, 20]; this is discussed below.

A very important multiwavelet system was constructed by J. Geronimo, D. Hardin, and P. Massopust [12] (see [1] for another early multiwavelet construction). Their system contains the two scaling functions

$\phi_1(t), \phi_2(t)$ shown in Figure 1 and the two wavelets $w_1(t), w_2(t)$ shown in Figure 2. The dilation and wavelet equations for this system have four coefficients:

$$\Phi(t) = \begin{bmatrix} \phi_1(t) \\ \phi_2(t) \end{bmatrix} = C[0]\Phi(2t) + C[1]\Phi(2t-1) + C[2]\Phi(2t-2) + C[3]\Phi(2t-3)\,,$$

$$C[0] = \begin{bmatrix} \frac{3}{5} & \frac{4\sqrt{2}}{5} \\ -\frac{1}{10\sqrt{2}} & -\frac{3}{10} \end{bmatrix}, \qquad C[1] = \begin{bmatrix} \frac{3}{5} & 0 \\ \frac{9}{10\sqrt{2}} & 1 \end{bmatrix},$$

$$C[2] = \begin{bmatrix} 0 & 0 \\ \frac{9}{10\sqrt{2}} & -\frac{3}{10} \end{bmatrix}, \qquad C[3] = \begin{bmatrix} 0 & 0 \\ -\frac{1}{10\sqrt{2}} & 0 \end{bmatrix}; \tag{3}$$

$$W(t) = \begin{bmatrix} w_1(t) \\ w_2(t) \end{bmatrix} = D[0]\Phi(2t) + D[1]\Phi(2t-1) + D[2]\Phi(2t-2) + D[3]\Phi(2t-3)\,,$$

$$D[0] = \frac{1}{10}\begin{bmatrix} -\frac{1}{\sqrt{2}} & -3 \\ 1 & 3\sqrt{2} \end{bmatrix}, \qquad D[1] = \frac{1}{10}\begin{bmatrix} \frac{9}{\sqrt{2}} & -10 \\ -9 & 0 \end{bmatrix},$$

$$D[2] = \frac{1}{10}\begin{bmatrix} \frac{9}{\sqrt{2}} & -3 \\ 9 & -3\sqrt{2} \end{bmatrix}, \qquad D[3] = \frac{1}{10}\begin{bmatrix} -\frac{1}{\sqrt{2}} & 0 \\ -1 & 0 \end{bmatrix}. \tag{4}$$

There are four remarkable properties of the Geronimo-Hardin-Massopust scaling functions:

- They each have short support (the intervals [0, 1] and [0, 2]).
- Both scaling functions are symmetric, and the wavelets form a symmetric/antisymmetric pair.
- All integer translates of the scaling functions are orthogonal.
- The system has second order of approximation (locally constant and locally linear functions are in V_0).

Let us stress that a scalar system with one scaling function cannot combine symmetry, orthogonality, and second order approximation. Moreover, a solution of a scalar dilation equation with four coefficients is supported on the interval [0, 3]!

Another useful multiwavelet pair is the symmetric pair determined by the three coefficients

$$C[0] = \begin{bmatrix} 0 & \frac{2+\sqrt{7}}{4} \\ 0 & \frac{2-\sqrt{7}}{4} \end{bmatrix}, \quad C[1] = \begin{bmatrix} \frac{3}{4} & \frac{1}{4} \\ \frac{1}{4} & \frac{3}{4} \end{bmatrix}, \quad C[2] = \begin{bmatrix} \frac{2-\sqrt{7}}{4} & 0 \\ \frac{2+\sqrt{7}}{4} & 0 \end{bmatrix}.$$

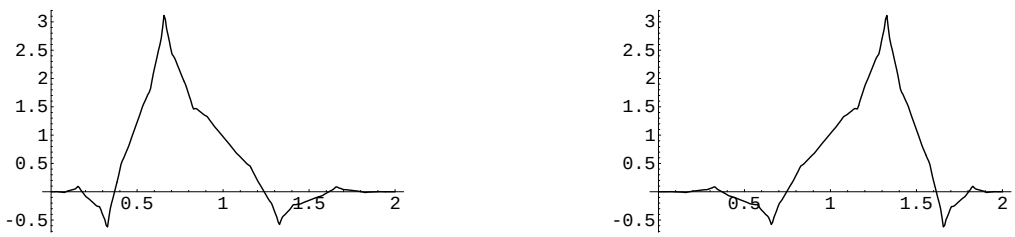

Figure 3: Symmetric pair of orthogonal multiwavelet scaling functions.

The scaling functions for this multiwavelet system are shown in Figure 3; observe that one is the reflection of the other about its center point. In this article we will make use of several other *nonsymmetric* multiwavelets with desirable properties.

Additional constructions of multiwavelets are given in [1, 9, 28, 29, 21, 17].

3 Multiwavelets and multirate filter banks

Corresponding to each multiwavelet system is a matrix-valued multirate filter bank [11], or multifilter. A multiwavelet filter bank [26] has "taps" that are $N \times N$ matrices (in this paper, we will be working with $N = 2$). Our principal example is the 4-coefficient symmetric multiwavelet filter bank whose lowpass filter was reported in [12]. This filter is given by the four 2×2 matrices $C[k]$ of equation (3). Unlike a scalar 2-band paraunitary filter bank, the corresponding highpass filter (specified by the four 2×2 matrices $D[k]$ of equation (4)) cannot be obtained simply as an "alternating flip" of the lowpass filter; the wavelet filters $D[k]$ must be designed [26]. The resulting 2-channel, 2×2 matrix filter bank operates on *two* input data streams, filtering them into *four* output streams, each of which is downsampled by a factor of 2. This is shown in Figure 4. Each row of the multifilter is a combination of two ordinary filters, one operating on the first data stream and the other operating on the second. For example, the first lowpass multiwavelet filter given in (3) operates as $c_{0,0}[k]$ on the first input stream and $c_{0,1}[k]$ on the second. It is a combination of the Haar filter $\{1, 1\}$ on the first stream and the unit impulse response on the second stream.

We ask that the matrix filter coefficients satisfy the orthogonality ("block-paraunitarity") condition

$$\sum_{k=0}^{N-1} C[k]\, C[k-2l]^T = 2\delta_{0,l}\, I \ . \tag{5}$$

In the time domain, filtering followed by downsampling is described by an infinite lowpass matrix with

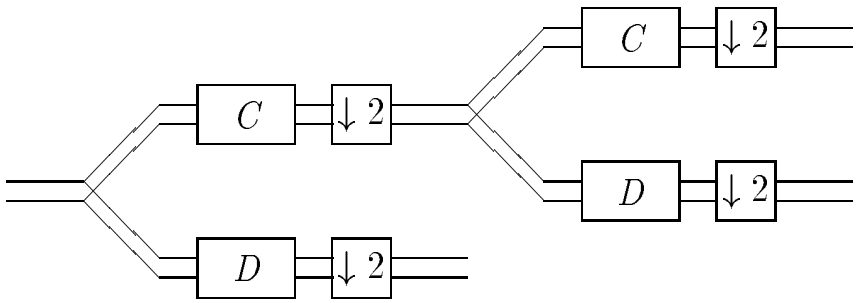

Figure 4: A multiwavelet filter bank, iterated once.

double shifts:

$$L = \begin{bmatrix} \cdots & & & & & & & \\ & C[3] & C[2] & C[1] & C[0] & 0 & 0 & \\ & 0 & 0 & C[3] & C[2] & C[1] & C[0] & \\ & & & & & & & \cdots \end{bmatrix} .$$

Each of the filter taps $C[k]$ is a 2×2 matrix. The eigenvalues of the matrix L are critical. The solution to the matrix dilation equation (1) is a two-element vector of scaling functions $\Phi(t) = [\phi_1(t), \phi_2(t)]^T$. The span of integer translates of the multiwavelet scaling functions is the "lowpass" space V_0, the set of *scale-limited signals* [13]. Any continuous-time function $f(t)$ in V_0 can be expanded as a linear combination

$$f(t) = \sum_n v_{1,n}^{(0)} \phi_1(t-n) + v_{2,n}^{(0)} \phi_2(t-n) .$$

The superscript (0) denotes an expansion "at scale level 0." $f(t)$ is completely described by the sequences $\left\{v_{1,n}^{(0)}\right\}$, $\left\{v_{2,n}^{(0)}\right\}$. Given such a pair of sequences, their coarse approximation (component in V_{-1}) is computed with the lowpass part of the multiwavelet filter bank:

$$\begin{bmatrix} \vdots \\ \begin{bmatrix} v_{1,n}^{(-1)} \\ v_{2,n}^{(-1)} \end{bmatrix} \\ \begin{bmatrix} v_{1,n+1}^{(-1)} \\ v_{2,n+1}^{(-1)} \end{bmatrix} \\ \vdots \end{bmatrix} = L \begin{bmatrix} \vdots \\ \begin{bmatrix} v_{1,n}^{(0)} \\ v_{2,n}^{(0)} \end{bmatrix} \\ \begin{bmatrix} v_{1,n+1}^{(0)} \\ v_{2,n+1}^{(0)} \end{bmatrix} \\ \vdots \end{bmatrix} .$$

Because the multifilter $C[k]$ is FIR, each apparently infinite sum in the matrix multiplication is actually finite and well-defined. Analogously, the details $w_{1,n}^{(-1)}$, $w_{2,n}^{(-1)}$ in W_{-1} are computed with the highpass part $D[k]$. Thus the multiwavelet filter bank plays the same mediating role in multiresolution analysis that a scalar filter bank plays for scalar wavelet systems. If the matrix L has eigenvalues $1, \frac{1}{2}, \ldots, \frac{1}{2^{p-1}}$ and the corresponding eigenvectors have a special form, then polynomials of degree less than p belong

to the space V_0 [14, 20]. This holds for the Geronimo-Hardin-Massopust multiwavelet filter with $p = 2$; linear functions can be exactly represented as linear combinations of integer translates of the scaling functions ϕ_1 and ϕ_2.

4 One-dimensional signal processing with multiwavelet filter banks

The lowpass filter C and highpass filter D consist of coefficients corresponding to the dilation equation (1) and wavelet equation (2). But in the multiwavelet setting these coefficients are n by n matrices, and during the convolution step they must multiply vectors (instead of scalars). This means that multifilter banks *need n input rows.* We will consider several ways to produce those rows. In this section the signals are one-dimensional; in the next section we consider two-dimensional signal processing.

4.1 Oversampled scheme

The most obvious way to get two input rows from a given signal is to repeat the signal. Two identical rows go into the multifilter bank. This procedure, which we call "repeated row," is shown in Figure 5. It introduces oversampling of the data by a factor of two. Oversampled representations require more calculation than critically-sampled representations. Furthermore, in data compression applications, one is seeking to remove redundancy, not increase it. In the case of one-dimensional signals the "repeated row" scheme is convenient to implement, and our experiments on denoising of one-dimensional signals were encouraging (see Section 6.1). In two dimensions the oversampling factor increases to four, making this scheme useful only for applications such as denoising which do not require critically-sampled or near-critically-sampled representation of the data.

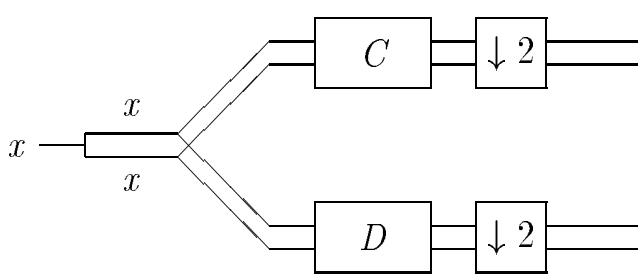

Figure 5: Multiwavelet filter bank with "repeated row" inputs.

4.2 A critically-sampled scheme: approximation-based preprocessing

A different way to get input rows for the multiwavelet filter bank is to *preprocess* the given scalar signal $f[n]$. For data compression, where one is trying to find compact transform representations for a dataset, it is imperative to find critically sampled multiwavelet transform schemes. We describe a

preprocessing scheme based on the approximation properties of the continuous-time multiwavelets which yields a critically sampled signal representation. This scheme (suggested to us by J. Geronimo) is naturally connected with the Geronimo-Hardin-Massopust multiwavelets.

Let the continuous-time function $f(t)$ belong to the scale-limited subspace V_0 generated by translates of the GHM scaling functions. This means that $f(t)$ is a linear combination of translates of those functions:

$$f(t) = \sum_n v_{1,n}^{(0)}\, \phi_1(t-n) + v_{2,n}^{(0)}\, \phi_2(t-n)\ . \tag{6}$$

Suppose that the input sequence $f[n]$ contains samples of $f(t)$ at half integers:

$$f[2n] = f(n), \qquad f[2n+1] = f(n+1/2).$$

$\phi_1(t)$ vanishes at all integer points. $\phi_2(t)$ is nonzero only at the integer 1. Sampling the relation (6) at integers and half integers gives

$$\begin{aligned} f[2n] &= \phi_2(1)\, v_{2,n-1}^{(0)}\,, \\ f[2n+1] &= \phi_2(3/2)\, v_{2,n-1}^{(0)} + \phi_1(1/2)\, v_{1,n}^{(0)} + \phi_2(1/2)\, v_{2,n}^{(0)}. \end{aligned} \tag{7}$$

The coefficients $v_{1,n}^{(0)}$, $v_{2,n}^{(0)}$ can be easily found from (7):

$$\begin{aligned} v_{1,n}^{(0)} &= \tfrac{\phi_2(1)\, f[2n+1] - \phi_2(1/2)\, f[2n+2] - \phi_2(3/2)\, f[2n]}{\phi_2(1)\, \phi_1(1/2)}\,, \\ v_{2,n}^{(0)} &= \tfrac{f[2n+2]}{\phi_2(1)}. \end{aligned}$$

Taking into account the symmetry of $\phi_2(t)$, we finally get

$$\begin{aligned} v_{1,n}^{(0)} &= \tfrac{\phi_2(1)\, f[2n+1] - \phi_2(1/2)\,(f[2n+2] + f[2n])}{\phi_2(1)\, \phi_1(1/2)}\,, \\ v_{2,n}^{(0)} &= \tfrac{f[2n+2]}{\phi_2(1)}\ . \end{aligned} \tag{8}$$

The relations (8) give a natural way to get two input rows $v_{1,n}^{(0)}$, $v_{2,n}^{(0)}$ starting from a given signal $f[n]$. To synthesize the signal on output we invert (8) and recover (7). This sequence of operations is depicted in Figure 6.

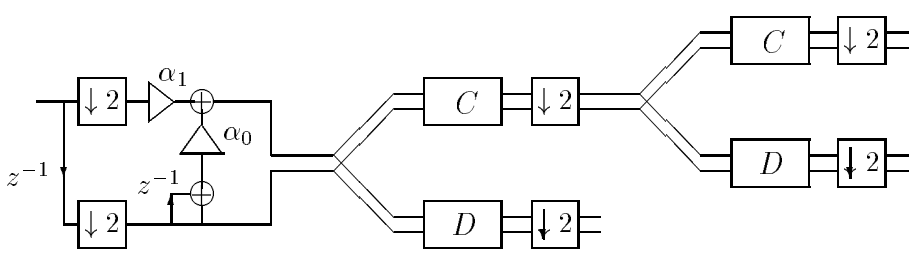

Figure 6: Approximation-based preprocessing and two steps of filtering for one-dimensional signals.

Given any $f(t) \in V_0$, the preprocessing step (8) followed by filtering will produce nontrivial output in the lowpass branch only. It yields zero output in the highpass subband. For example, $f(t) \equiv 1$ (locally in V_0) gives $v_{1,n}^{(0)} = 1$ and $v_{2,n}^{(0)} = \sqrt{2}$, which is the eigenvector of the matrix L^T with eigenvalue 1.

This preprocessing algorithm also maintains a critically sampled representation: if the data enters at rate R, preprocessing yields two streams at rate $R/2$ for input to the multifilter, which produces four output streams, each at a rate $R/4$.

Another advantage of this approximation-based preprocessing method is that it fits naturally with symmetric extension for multiwavelets (discussed below in Subsection 4.3). In other words, if we symmetrically extend a finite length signal $f[n]$ at its boundaries and implement the approximation formulas (8), then the two rows $v_{1,n}^{(0)}, v_{2,n}^{(0)}$ from the preprocessor will have the appropriate symmetry.

One also can develop a general approximation-type preprocessing based on the following idea. Suppose again that our given signal f lies in V_0. This implies that

$$f(t) = \sum_{n,k} v_{k,n}^{(0)} \phi_k(t-n). \tag{9}$$

The goal of preprocessing is to find the coefficients $v_{k,n}^{(0)}$ from the signal samples.

For the beginning we assume that our multiwavelet system has N scaling functions, all supported on $[0,1]$. Now restrict equation (9) to this interval:

$$f(t) = \sum_{k} v_{k,0}^{(0)} \phi_k(t) \ , \qquad 0 \le t \le 1. \tag{10}$$

Suppose that samples $f[0], \ldots, f[N-1]$ are the values of the function $f(t)$ at the points

$$t = \frac{1}{2N}, \frac{3}{2N}, \ldots, \frac{2N-1}{2N}.$$

The representation (10) gives a linear system for the coefficients $v_{0,0}^{(0)}, \ldots, v_{N-1,0}^{(0)}$. The following N samples $f[N], \ldots, f[2N-1]$ give the values of $v_{0,1}^{(0)}, \ldots, v_{N-1,1}^{(0)}$. Repeating this procedure we find all the $v_{k,n}^{(0)}$. If some of the scaling functions have support longer than $[0,1]$, we will need several initial (boundary) values of $v_{k,-1}^{(0)}, v_{k,-2}^{(0)}, \ldots$. In the case of finite length signals, these numbers can be obtained from the conditions of periodization or symmetric extension (Section 4.3). Other multiwavelet preprocessing techniques are discussed in [29], [31].

4.3 Symmetric extension of finite-length signals

In practice all signals have finite length, so we must devise techniques for filtering such signals at their boundaries. There are two common methods for filtering at the boundary that preserve critical sampling. The first is circular periodization (periodic wrap) of the data. This method introduces discontinuities at

the boundaries; however, it can be used with almost any filter bank. The second approach is symmetric extension of the data. Symmetric extension preserves signal continuity, but can be implemented only with linear-phase (symmetric and/or antisymmetric) filter banks [24, 3, 16, 4]. We now develop symmetric extension for linear-phase multiwavelet filters, such as the Geronimo-Hardin-Massopust multifilters. This proves useful for image compression applications (Section 6).

Recall the basic problem: given an input signal $f[n]$ with N samples and a linear-phase (symmetric or antisymmetric) filter, how can we symmetrically extend f before filtering and downsampling in a way that preserves the critically sampled nature of the system? The possibilities for such an extension have been enumerated in [4]. Depending on the parity of the input signal (even- or odd-length) and the parity and symmetry of the filter, there is a specific non-expansive symmetric extension of both the input signal and the subband outputs. For example, an even-length input signal passed through an even-length symmetric lowpass filter should be extended by repeating the first and last samples, i.e., a half-sample symmetric signal is matched to a half-sample-symmetric filter. Similarly, when the lowpass filter is of odd length (whole-sample-symmetry), the input signal should be extended without repeating the first or last samples.

Each row of the GHM multifilter (equations (3) and (4)) is a linear combination of two filters, one for each input stream. One filter (applied to the first stream) is of even length; the second is of odd length. Thus we should extend the first stream using half-sample-symmetry (repeating the first and last samples) and extend the second stream using whole-sample-symmetry (*not* repeating samples). Then, when synthesizing the input signal from the subband outputs, we must symmetrize the subband data differently depending on whether it is going into an even- or odd-length filter.

In particular suppose we are given two input rows (one of even length, the other of odd length):

$$\begin{matrix} v_{1,0}^{(0)} & v_{1,1}^{(0)} & v_{1,2}^{(0)} & \dots & v_{1,N-1}^{(0)} & \\ v_{2,0}^{(0)} & v_{2,1}^{(0)} & v_{2,2}^{(0)} & \dots & v_{2,N-1}^{(0)} & v_{2,N}^{(0)} \end{matrix} .$$

If they are symmetrically extended as

$$\begin{matrix} \dots & v_{1,1}^{(0)} & v_{1,0}^{(0)} & v_{1,0}^{(0)} & v_{1,1}^{(0)} & \dots \\ \dots & v_{2,1}^{(0)} & v_{2,0}^{(0)} & v_{2,1}^{(0)} & v_{2,2}^{(0)} & \dots \end{matrix} \tag{11}$$

at the start and

$$\begin{matrix} \dots & v_{1,N-2}^{(0)} & v_{1,N-1}^{(0)} & v_{1,N-1}^{(0)} & \dots \\ \dots & v_{2,N-1}^{(0)} & v_{2,N}^{(0)} & v_{2,N-1}^{(0)} & \dots \end{matrix} \tag{12}$$

at the end to give two symmetric rows, then after one step of the cascade algorithm we have the four

symmetric subband outputs:

$$\begin{array}{ccccccccc}
\dots & v_{1,1}^{(-1)} & v_{1,0}^{(-1)} & v_{1,0}^{(-1)} & \dots & v_{1,\frac{N}{2}-2}^{(-1)} & v_{1,\frac{N}{2}-1}^{(-1)} & v_{1,\frac{N}{2}-1}^{(-1)} & \dots \\
\dots & v_{2,1}^{(-1)} & v_{2,0}^{(-1)} & v_{2,1}^{(-1)} & \dots & v_{2,\frac{N}{2}-1}^{(-1)} & v_{2,\frac{N}{2}}^{(-1)} & v_{2,\frac{N}{2}-1}^{(-1)} & \dots \\
\dots & w_{1,1}^{(-1)} & w_{1,0}^{(-1)} & w_{1,1}^{(-1)} & \dots & w_{1,\frac{N}{2}-1}^{(-1)} & w_{1,\frac{N}{2}}^{(-1)} & w_{1,\frac{N}{2}-1}^{(-1)} & \dots \\
\dots & -w_{2,1}^{(-1)} & 0 & w_{2,1}^{(-1)} & \dots & w_{2,\frac{N}{2}-1}^{(-1)} & 0 & -w_{2,\frac{N}{2}-1}^{(-1)} & \dots
\end{array}$$

The application of the (linear-phase) multiwavelet synthesis filters now yields the symmetric extension of the original signal.

Multiwavelet symmetric extension can be done not only for linear-phase filters. For example, the symmetric pair of scaling functions shown in Figure 3 admits the following extension of input data rows $v_{1,k}^{(0)}$ and $v_{2,k}^{(0)}$:

$$\begin{array}{ccccccccccc}
\dots & v_{2,1}^{(0)} & v_{2,0}^{(0)} & a & v_{1,0}^{(0)} & v_{1,0}^{(0)} & v_{1,1}^{(0)} & \dots & v_{1,N-1}^{(0)} & a & v_{2,N-1}^{(0)} & \dots \\
\dots & v_{1,1}^{(0)} & v_{1,0}^{(0)} & a & v_{2,0}^{(0)} & v_{2,1}^{(0)} & v_{2,2}^{(0)} & \dots & v_{2,N-1}^{(0)} & a & v_{1,N-1}^{(0)} & \dots
\end{array}.$$

The placeholder a is an arbitrary real number. After filtering and downsampling of this extended data, the output rows will have the same symmetry. In this way we obtain a non-expansive transform of finite-length input data which behaves well at the boundaries under lossy quantization.

5 Two-dimensional signal processing with multiwavelet filter banks

Multiwavelet filtering of images needs two-dimensional algorithms. One class of such algorithms is derived simply by taking tensor products of the one-dimensional methods described in the previous section. Another class of algorithms stems from using the matrix filters of the multiwavelet system for fundamentally two-dimensional processing. We discuss each of these alternatives now.

5.1 Separable schemes based on one-dimensional methods

Section 4 described two different methods for transforming one-dimensional signals with multiwavelets. Each of these can be turned into a two-dimensional algorithm by taking a tensor product, i.e., by performing the 1D algorithm in each dimension separately. As noted before, the separable product of one-dimensional "repeated row" algorithms leads to a 4:1 data expansion, restricting the utility of this approach to applications such as denoising by thresholding, for which near-critical sampling is irrelevant.

The separable product of the approximation-based preprocessing methods described in Section 4.2 yields a critically sampled representation, potentially useful for both denoising and data compression.

However, this two-dimensional scheme is not trivial. If we approximate and transform with downsampling, a constant row $f[n] = 1$ would become two different halflength rows. (In the case of GHM scaling functions one row repeats the constant 1, and the other repeats the constant $\sqrt{2}$.) To overcome this, we *de-approximate* the multiwavelet filter bank output to create two output rows (one lowpass, one highpass) before operating in the vertical direction. The vertical transform similarly proceeds as approximate-filter-deapproximate before the next level of the cascade algorithm is applied. This is described schematically in Figure 7.

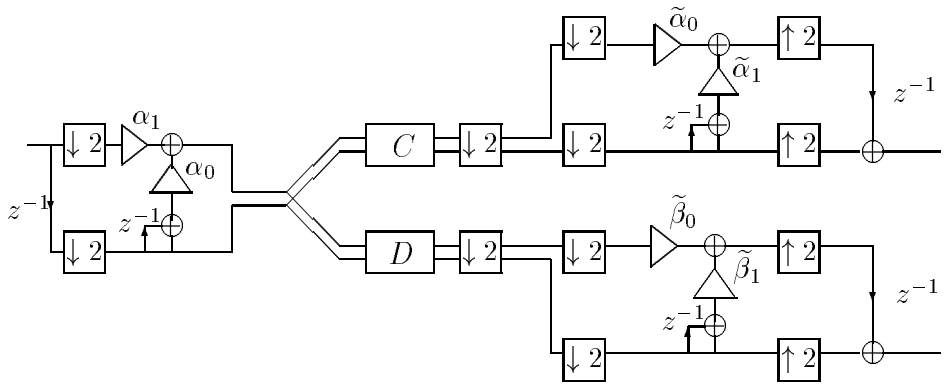

Figure 7: Approximation/de-approximation scheme for computing the 2-dimensional multiwavelet transform.

5.2 Constrained multiwavelets

A different approach to two-dimensional multiwavelet filtering is to make use of the two-dimensionality of the matrix filter coefficients. When processing an image with a scalar filterbank one usually uses as input the rows and columns of the image. For a multiwavelet system we need n input signals. Where can we get them? The first solution which comes to mind is very simple: just use n adjacent rows as the input. For the 2×2 multiwavelets used here, this would mean taking two rows of the image at a time, and applying the matrix filter coefficients to the sequence of 2-element vectors in the input stream.

However, a naive implementation of this approach does not lead to good results (see Table 4 in Section 6.4). This is due to the intricacies of multiwavelet approximation. Approximation of degree p is important for image compression because locally polynomial data can be captured in a few lowpass coefficients. A wavelet system (scalar or multiwavelet) satisfies approximation of degree p (or accuracy p) if polynomials of degree less than p belong to the scale-limited space V_0. Image data is often locally well-approximated by constant, linear, and quadratic functions; thus, such local approximations remain in the lowpass space V_0 after filtering and downsampling. This is one reason why simply retaining the lowpass coefficients of a wavelet decomposition with accuracy p (p vanishing moments) produces good results while compressing the image representation into very few coefficients [32].

When applying multiwavelets to two-dimensional (image) processing, we use this notion of local approximation as a motivation — we wish to capture locally constant and linear features in the lowpass coefficients. Suppose we have a multiwavelet system generated by two scaling functions $\phi_1(t), \phi_2(t)$ with accuracy $p \geq 1$ (this would mean at least one vanishing wavelet moment in the scalar case). Then constant functions $f(t) \equiv c$ locally belong to the scale-limited space V_0. It has been shown [14] that the repeated constant 1 is an eigenvalue of the filtering and downsampling operator L, and there exists a left eigenvector

$$[\mathbf{u}_n] = \left[\ \ldots u_{1,n} \ , \ u_{2,n} \ , \ u_{1,n+1} \ , \ u_{2,n+1} \ , \ \ldots \ \right]$$

with

$$[\mathbf{u}_n] \, L = [\mathbf{u}_n] \ .$$

In fact, $u_{1,n} = u_{1,0}$ and $u_{2,n} = u_{2,0}$, so that

$$\left[\ \ldots u_{1,n} \ , \ u_{2,n} \ , \ u_{1,n+1} \ , \ u_{2,n+1} \ , \ \ldots \ \right] = \left[\ \ldots u_{1,0} \ , \ u_{2,0} \ , \ u_{1,0} \ , \ u_{2,0} \ , \ \ldots \ \right] \ .$$

In the continuous-time subspace V_0 this eigenvector leads to the constant function:

$$f(t) = c = c \sum_n \left(u_{1,n} \phi_1(t-n) + u_{2,n} \phi_2(t-n) \right) \ .$$

Assuming for the moment that our image is locally constant, we input two equal, constant rows of the image (two-dimensional signal) into the multiwavelet filter bank. The output will be zero in the highpass and a constant vector

$$\begin{bmatrix} c_1 \\ c_2 \end{bmatrix}$$

in the lowpass. If the eigenvector $[\mathbf{u}_n]$ of L satisfies $u_{1,0} = u_{2,0}$, then we will get $c_1 = c_2$ and the constant input yields a constant lowpass output. However, there is no guarantee of this happy state; for example, in the case of the Geronimo-Hardin-Massopust multiwavelet (3),

$$[u_{1,0} \quad u_{2,0}] \propto \begin{bmatrix} 1 & \sqrt{2} \end{bmatrix}$$

and therefore $c_1 \neq c_2$. Thus the lowpass responses of an arbitrary multifilter to a constant input are *different* constants. Quantization of these lowpass multifilter outputs (for lossy compression) will then introduce a rippled texture in the lowpass part of the image, creating unacceptable artifacts. This is borne out by experiments using the GHM multifilter (Section 6.4 below).

Similar arguments hold for linear approximation [14]: a multiwavelet system has linear approximation (accuracy of order $p = 2$) if and only if there are two left eigenvectors. The first is

$$[\mathbf{u}_n] = \left[\ \ldots \ u_{1,0} \ , \ u_{2,0} \ , \ u_{1,0} \ , \ u_{2,0} \ , \ \ldots \ \right]$$

satisfying

$$[\mathbf{u}_n]\, L = [\mathbf{u}_n] \ .$$

as before. The second eigenvector is

$$[\mathbf{v}_n] = \left[\ \ldots v_{1,n} \ , \ v_{2,n} \ , \ v_{1,n+1} \ , \ v_{2,n+1} \ , \ \ldots \ \right]$$

also satisfying

$$[\mathbf{v}_n]\, L = [\mathbf{v}_n] \ .$$

For linear approximation we must have

$$v_{1,n} = y_{1,0} - n u_{1,0}$$

and

$$v_{2,n} = y_{2,0} - n u_{2,0}$$

for some constants $y_{1,0}$ and $y_{2,0}$, so that

$$[\mathbf{v}_n] = \left[\ \ldots y_{1,0} - n u_{1,0} \ , \ y_{2,0} - n u_{2,0} \ , \ y_{1,0} - (n+1) u_{1,0} \ , \ y_{2,0} - (n+1) u_{2,0} \ , \ \ldots \ \right] \ .$$

This second eigenvector leads to linear approximation; indeed,

$$g(t) = t = \sum_n v_{1,n} \phi_1(t-n) + v_{2,n} \phi_2(t-n) \ .$$

Again, there is no reason to expect that $y_{1,0} = y_{2,0}$, and so if we input two equal linear rows into the multifilter, they will most likely emerge as two *different* linear rows. Thus the locally linear nature of many images will become distorted under such a multiwavelet transform, and this distortion will lead to unacceptable artifacts under quantization.

One way to avoid this phenomenon is to construct a multiwavelet system in which the eigenvectors have pairwise equal components

$$[\mathbf{u}_n] = \left[\ \ldots u_{1,0} \ , \ u_{1,0} \ , \ u_{1,0} \ , \ \ldots \ \right] \tag{13}$$

and

$$[\mathbf{v}_n] = \left[\ \ldots y_{1,0} - n u_{1,0} \ , \ y_{1,0} - n u_{1,0} \ , \ y_{1,0} - (n+1) u_{1,0} \ , \ y_{1,0} - (n+1) u_{1,0} \ , \ \ldots \ \right] \ , \tag{14}$$

which produces two equal linear outputs as the response to two equal linear inputs. Such multiwavelets can be constructed, but as we will see, the restrictions (13) and (14) imply some constraints on the properties of the multiscaling functions.

Consider a multiwavelet system with two scaling functions satisfying a matrix dilation equation with four coefficients

$$\Phi(t) = \begin{bmatrix} \phi_1(t) \\ \phi_2(t) \end{bmatrix} \tag{15}$$

$$= C[0]\Phi(2t) + C[1]\Phi(2t-1) + C[2]\Phi(2t-2) + C[3]\Phi(2t-3) .$$

It is proven in [14] that the vectors $u = [u_{1,0} \quad u_{2,0}]$, $y = [y_{1,0} \quad y_{2,0}]$ must satisfy the following system of equations:

$$\begin{aligned} u\,(C[0]+C[2]) &= u \\ u\,(C[1]+C[3]) &= u \\ yC[1]+(u+y)C[3] &= \tfrac{1}{2}y \\ yC[0]+(u+y)C[2] &= \tfrac{1}{2}(u+y) . \end{aligned} \tag{16}$$

We want

$$u_{1,0} = u_{2,0} = u_0 , \tag{17}$$

and

$$y_{1,0} = y_{2,0} = y_0 , \tag{18}$$

i.e., $y = (y_0/u_0)\,u$. From the dilation equation (15) and the approximation constraints (16), it follows that u is a mutual eigenvector of all four matrices $C[k]$:

$$u\,C[k] = c'_k u,\ k = 0,\ 1,\ 2,\ 3 . \tag{19}$$

Consider now a scalar function $\phi(t)$

$$\phi(t) = \frac{1}{u_0} u\,\Phi(t) = \phi_1(t) + \phi_2(t).$$

According to (15) and (19), $\phi(t)$ satisfies the scalar dilation equation

$$\phi(t) = c'_0\phi(2t) + c'_1\phi(2t-1) + c'_2\phi(2t-2) + c'_3\phi(2t-3).$$

The only solution to this equation with orthogonal translates and second order of approximation is Daubechies' D_4 scaling function [6]. Thus any orthogonal pair $\{\phi_1\,,\ \phi_2\}$ which has second order of approximation, satisfies the dilation equation (15), and the eigenvector constraints (17) — (18) must sum to D_4:

$$\phi_1(t) + \phi_2(t) = D_4(t).$$

We call such pairs "constrained" multiscaling functions. There are infinitely many constrained orthogonal solutions of (19). Plots of two of them are shown in Figures 8 and 9.

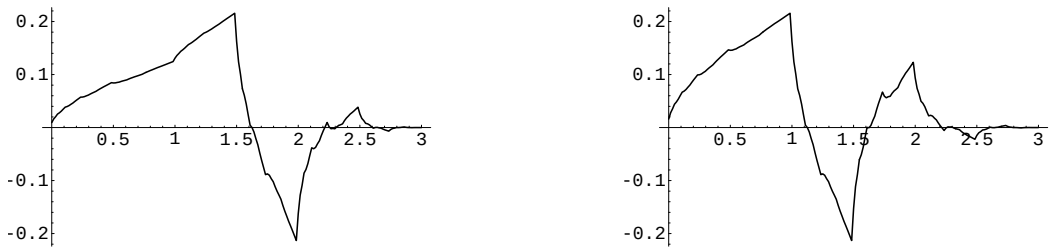

Figure 8: Constrained Pair 1.

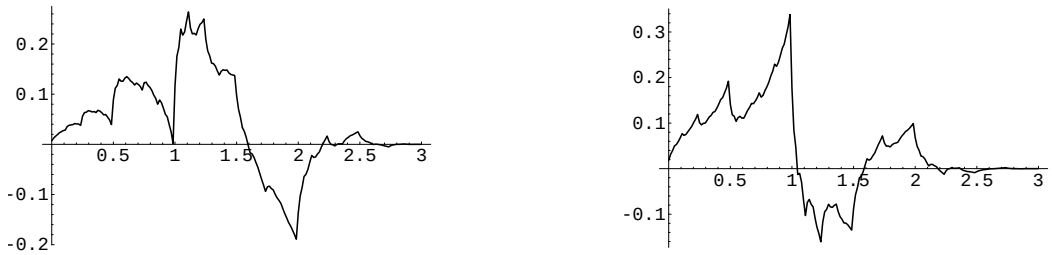

Figure 9: Constrained Pair 2.

The implementation of constrained multiwavelets for the two-dimensional wavelet transform is straightforward. In each step of Mallat's algorithm [18], one first processes pairs of rows and then pairs of columns. Because locally constant and linear data are passed through to the lowpass ouputs of a constrained multifilter, the performance of these constrained multiwavelets in image compression is much better than that of the "non-constrained" GHM pair, when applied by using two adjacent rows as the input. This is confirmed by the experiments reported in the next section, as shown in Tables 4 and 5.

6 Signal processing applications of multiwavelets

In this section we are going to compare the numerical performance of GHM and constrained multiwavelets with Daubechies D_4 scalar wavelets. D_4 wavelets were chosen because they have two vanishing moments, are orthogonal and have four coefficients in the dilation equation — exactly like the GHM and constrained pairs. We perform these comparisons in two standard wavelet applications: signal denoising and data compression. We first develop these applications for one-dimensional signals, then extend them to images.

6.1 Denoising by soft thresholding

Suppose that a signal of interest f has been corrupted by noise, so that we observe a signal g:

$$g[n] = f[n] + \sigma z[n],$$

where $z[n]$ is unit-variance, zero-mean Gaussian white noise. What is a robust method for recovering f from the samples $g[n]$ as best as possible? Donoho and Johnstone [7, 8] have proposed a solution via wavelet shrinkage or soft thresholding in the wavelet domain. Wavelet shrinkage works as follows:

1. Apply the cascade algorithm to get the wavelet coefficients corresponding to $g[n]$.
2. Choose a threshold $t_n = \sqrt{2\log(n)}\gamma\sigma/\sqrt{n}$ and apply (soft) thresholding to the wavelet coefficients.
3. Invert the cascade algorithm to get the denoised signal $\hat{f}[n]$.

Donoho and Johnstone's algorithm offers the advantages of smoothness and adaptation. Wavelet shrinkage is *smooth* in the sense that the denoised estimate $\hat{f}$ has a very high probability of being as smooth as the original signal f, in a variety of smoothness spaces (Sobolev, Hölder, etc.). Wavelet shrinkage also achieves near-minimax mean-square-error among possible denoisings of f, measured over a wide range of smoothness classes. In these numerical senses, wavelet shrinkage is superior to other smoothing and denoising algorithms. Heuristically, wavelet shrinkage has the advantage of not adding "bumps" or false oscillations in the process of removing noise, because of the local and smoothness-preserving nature of the wavelet transform. Wavelet shrinkage has been successfully applied to SAR imagery as a method for clutter removal [19]. It is natural to attempt to use multiwavelets as the transform for a wavelet shrinkage approach to denoising, and compare the results with scalar wavelet shrinkage.

We implemented Donoho's wavelet shrinkage algorithm using several additional remarks from [19]. We compared the performance of the D_4 scalar wavelet transform with oversampled and critically sampled multiwavelet schemes. In the oversampled scheme, the first row is multiplied by $\sqrt{2}$, to better match the first eigenvector of the GHM system. The critically sampled scheme uses the formulas (8) to obtain two input rows $v_{1,n}$, $v_{2,n}$ from a single row of data. After reconstruction the two output rows $\hat{v}_{1,n}$, $\hat{v}_{2,n}$ are deapproximated using (7), to yield the output signal $\hat{f}[n]$. Boundaries are handled by symmetric data extension for the critically sampled (approximation/deapproximation) and oversampled schemes, and by circular periodization for D_4.

Results of a typical experiment are shown in Table 6.1 and Figure 10. In all experiments both types of GHM filter banks performed better than D_4. The "repeated row" usually gave better results than "approximation" preprocessing. This is not surprising, because it is known that oversampled data representations are useful for feature extraction.

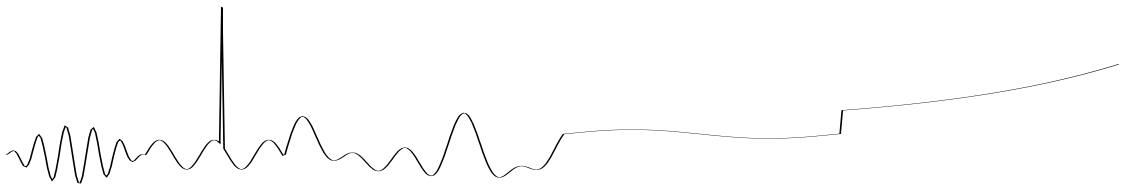

Original signal, 512 samples. Range of amplitude $[-3, 10]$

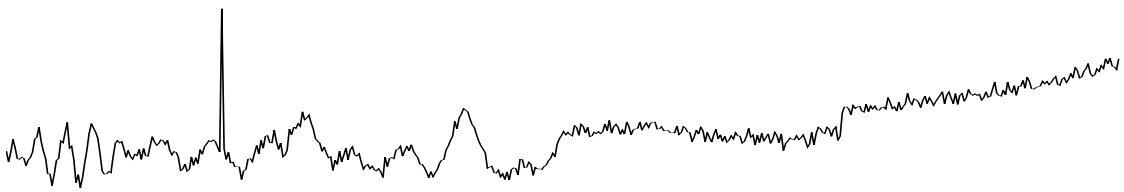

Noisy signal. Noise level $\sigma = 0.3$

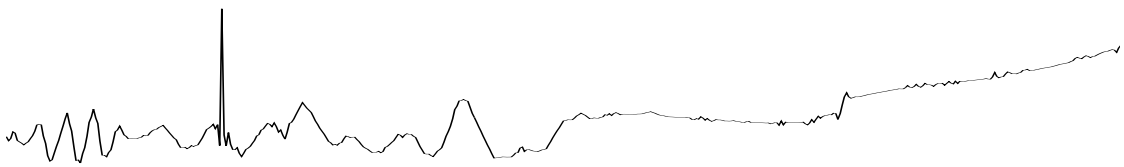

Signal reconstructed using GHM with "approximation".

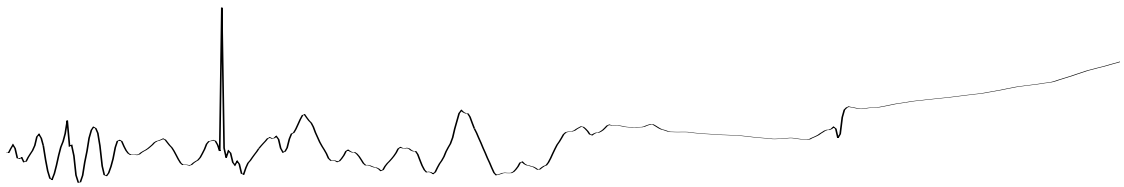

Signal reconstructed using GHM with "repeated row".

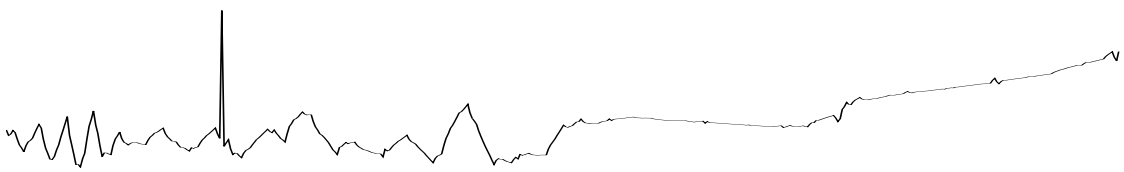

Signal reconstructed using D_4.

Figure 10: Denoising via wavelet-shrinkage

	Noise	GHM with approximation	GHM with repeated row	D_4
mean abs. error	0.243	0.154	0.128	0.213
mean square error	0.093	0.045	0.029	0.062

Table 1: Denoising via wavelet soft thresholding

6.2 Thresholding for compression of one-dimensional signals

We also performed a model compression experiment, using the same one-dimensional signal as in the denoising experiments. We applied seven iterations of the cascade algorithm on this 512-point signal to get the wavelet coefficients λ_k, using the same three types of wavelet and multiwavelet filter banks. For a fair comparison, we retained the same number of the largest coefficients for each transform, then inverted the cascade algorithm to reconstruct the signal. The results are shown in Table 2 and Figure 11.

	GHM with "appr."	GHM with "rep. row"	D_4
recon with 50 largest coeffs.			
ℓ^1 error	0.1298	0.1597	0.1807
ℓ^2 (mean square) error	0.0448	0.0517	0.0815
ℓ^∞ (maximum) error	1.5709	1.0667	1.4923
recon with 75 largest coeffs.			
ℓ^1 error	0.0601	0.0650	0.0890
ℓ^2 (mean square) error	0.0091	0.0107	0.0200
ℓ^∞ (maximum) error	0.7959	0.9731	0.7301
recon with 100 largest coeffs.			
ℓ^1 error	0.0320	0.0389	0.0466
ℓ^2 (mean square) error	0.0029	0.0030	0.0049
ℓ^∞ (maximum) error	0.2821	0.2309	0.2867

Table 2: One-dimensional compression by retention of largest coefficients.

For a given number of retained coefficients, the multiwavelet transforms lead to smaller ℓ^1 and ℓ^2 (mean-square) errors than the D_4 scalar wavelet transform, and comparable ℓ^∞ (maximum) errors. GHM with "approximation" is slightly superior to GHM with "repeated row". The results of this experiment led us to try using the GHM multiwavelet with "approximation" for two-dimensional image compression (with a true quantizer and coder), as discussed in Section 6.4 below.

Original signal, 512 samples. Range of amplitude $[-3, 10]$

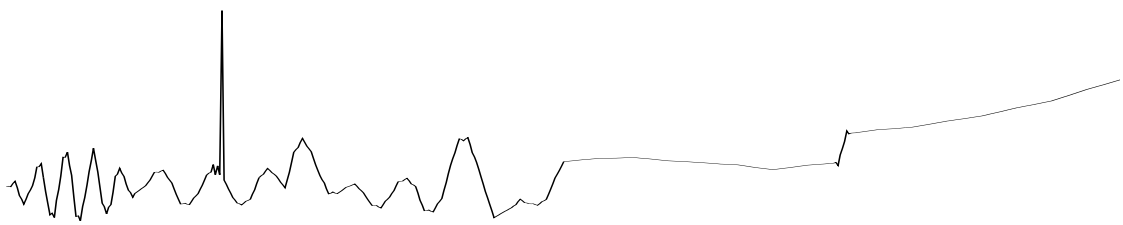

Reconstruction from 75 largest coeffs of GHM with "approximation".

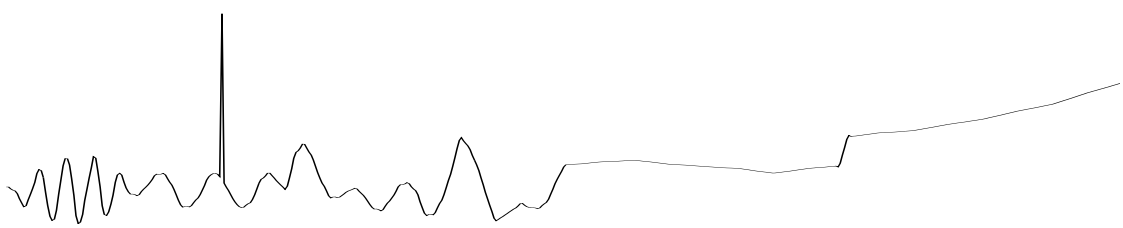

Reconstruction from 75 largest coeffs of GHM with "repeated row".

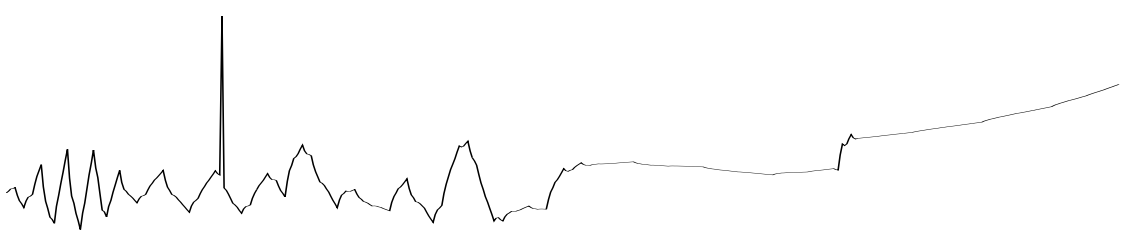

Reconstruction from 75 largest coeffs of D_4 **transform.**

Figure 11: One-D signal compression via retention of large coefficients.

6.3 Denoising of images

Given the success of the multiwavelet system in denoising of the model one-dimensional signal, we applied multiwavelet denoising to imagery. We added white Gaussian noise to the *Lenna* image, and applied three wavelet transforms for denoising by wavelet shrinkage: the GHM multiwavelet with approximation, GHM with repeated row, and the Daubechies 4-tap scalar wavelet. The experimental results are shown in Table 3 and the resulting images in Figure 12. The GHM multiwavelet with approximation was superior to D_4 both numerically and subjectively; the approximation-based preprocessing seemed to reduce the Cartesian artifacts present in the scalar wavelet shrinkage. This can be seen, for example, in the facial features (eyes, nose) of the *Lenna* images shown in Figure 12. The GHM-repeated row scheme suffered because we had to repeat rows in first the x dimension and then in the y dimension, altering the correlations of the data. This produces the broad stripes in the image denoised with the repeated row scheme.

	Noise	GHM with approximation	GHM with repeated row	D_4
ℓ^1 error	19.93	6.87	9.70	8.09
ℓ^2 error	24.98	9.75	12.6	11.4

Table 3: Denoising of *Lenna* image via wavelet-shrinkage.

6.4 Transform-based image coding

One of the most successful applications of the wavelet transform is image compression. A transform-based coder operates by transforming the data to remove redundancy, then quantizing the transform coefficients (a lossy step), and finally entropy coding the quantizer output. Because of their energy compaction properties and correspondence with the human visual system, wavelet representations have produced superior objective and subjective results in image compression [18, 32, 2, 5]. Since a wavelet basis consists of functions with short support (for high frequencies) and long support (for low frequencies), large smooth areas of an image may be represented with very few bits, and detail added where it is needed. Multiwavelet decompositions offer all of these traditional advantages of wavelets, as well as the combination of orthogonality, short support, and symmetry. The short support of multiwavelet filters limits ringing artifacts due to subsequent quantization. Symmetry of the filter bank both leads to efficient boundary handling and preserves centers of mass, lessening the blurring of fine-scale features. Orthogonality is useful because it means that rate-distortion optimal quantization strategies may be employed in the transform domain and still lead to optimal time-domain quantization (at least when error is measured in a mean-square sense). Thus it is natural to consider the use of multiwavelets in a transform-based image coder.

Lenna image with Gaussian noise
MSE 24.98

GHM-with-approximation
multiwavelet denoising, MSE 9.75

Daubechies 4 scalar
wavelet denoising, MSE 11.4

GHM-repeated-row
multiwavelet denoising, MSE 12.6

Figure 12
Multiwavelet denoising

Figure 12: Postscript version of glossy photo attachment

We compared the two-dimensional multiwavelet algorithms of Section 5 with a D_4 scalar wavelet in a production image coding system. Five types of wavelet transform were used:

- D_4 scalar wavelet
- Approximation/deapproximation preprocessing with GHM multiwavelets
- Adjacent rows input with GHM multiwavelets
- Adjacent rows input with symmetric pair
- Adjacent rows input with two different constrained pairs

Each of these wavelet transforms was followed by entropy-constrained scalar quantization and entropy coding. We made the assumption that the histograms of subband (or wavelet transform subblock) coefficient values obeyed a Laplacian distribution [18], and designed a uniform scalar quantizer. The quantizer optimized the bit allocation among the different subbands by using an operational rate-distortion approach (minimizing the functional $D + \lambda R$) [23]. We then entropy-coded the resulting coefficient streams using a combination of zero-run-length coding and adaptive Huffman coding, as in the FBI's Wavelet Scalar Quantization standard [10].

We applied these different wavelet image coders to the Lenna (NITF6) image, as well as a geometric test pattern, at a variety of compression ratios. The results are shown in Tables 4 and 5, and in Figures 13 and 14. On Lenna, the GHM multiwavelet with approximation mildly outperformed the D_4 scalar wavelet at compression ratios of 32:1 and 64:1. The images in Figure 13 show that the GHM-approximation scheme preserves more texture in the hat and, as in the denoising application, produce fewer Cartesian artifacts than the scalar wavelet scheme. The repeated-row method did not work well on *Lenna*. However, the repeated-row method produced the best compressions of the test pattern image (14) at intermediate compression ratios (16:1 and 32:1), with the constrained pair #1 "CP-1" outperforming both D_4 and GHM with approximation. When using the repeated row algorithm, the constrained pairs significantly outperformed the GHM symmetric multiwavelet, demonstrating the importance of the eigenvector constraints (13 - 14). A close look at the details of the compressed/decompressed test patterns shows that the CP-1 compression did a better job of preserving the checkerboard and "rang" over a shorter distance than the D_4 compression. The alteration of the checkerboard pattern in the D_4 compression may be due to the lack of linear-phase symmetry in the wavelet filters.

These preliminary results suggest that multiwavelets are worthy of further investigation as a technique for image compression. Issues to address include the design of multiwavelets with symmetry and higher order of approximation than the GHM system, the role of eigenvector constraints, and also further

exploration of regularity for multiwavelets [30]. One might also apply zerotree-coding methods [22] in a multiwavelet context.

Compression Ratio	8:1	16:1	32:1	64:1
	pSNR	pSNR	pSNR	pSNR
Daubechies 4	35.6	32.3	29.3	26.8
GHM with appr./deappr.	35.3	31.8	29.4	27.1
Adjacent Row Processing:				
GHM	24.1	21.3	19.7	18.4
symmetric pair	31.1	27.3	24.0	21.8
constrained pair #1	32.4	28.5	25.1	23.0
constrained pair #2	31.9	28.2	25.0	22.8

Table 4: Peak SNRs for compression of *Lenna*.

Compression Ratio	8:1	16:1	32:1	64:1
	pSNR	pSNR	pSNR	pSNR
Daubechies 4	48.5	31.4	23.0	19.8
GHM with appr./deappr.	52.4	34.0	18.3	16.8
Adjacent Row Processing:				
GHM	29.8	25.4	20.1	15.8
symmetric pair	33.3	28.3	20.9	16.5
constrained pair 1	42.2	32.3	23.9	19.0
constrained pair 2	33.3	30.2	21.6	17.6

Table 5: Peak SNRs for compression of geometric test pattern.

Lenna original

GHM approximation-based
multiwavelet compression
64:1, pSNR 27.1

Daubechies 4
scalar wavelet compression
64:1, pSNR 26.8

Constrained-Pair #1
multiwavelet compression
64:1, pSNR 23.0

Figure 13
Multiwavelet compression

Figure 13: Postscript version of glossy photo attachment

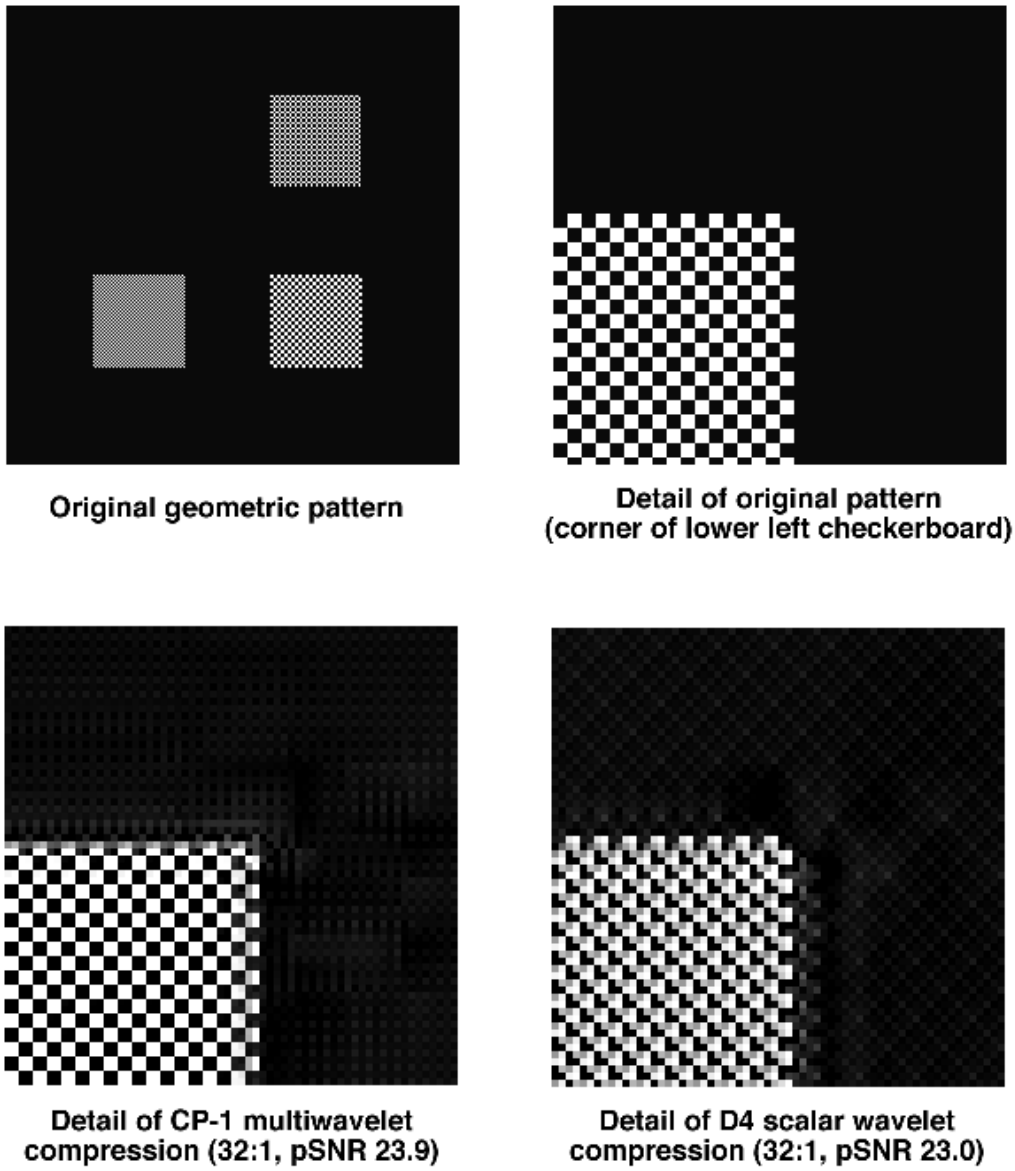

Figure 14
Multiwavelet compression

Figure 14: Postscript version of glossy photo attachment

7 Conclusions

After reviewing the recent notion of multiwavelets (matrix-valued wavelet systems), we have examined the use of multiwavelets in a filter bank setting for discrete-time signal processing. Multiwavelets offer the advantages of combining symmetry, orthogonality, and short support, properties not mutually achievable with scalar 2-band wavelet systems. However, multiwavelets differ from scalar wavelet systems in requiring two or more input streams to the multiwavelet filter bank. We described two methods (repeated row and approximation/deapproximation) for obtaining such a vector input stream from a one-dimensional signal. We developed the theory of symmetric extension for multiwavelet filter banks, which matches nicely with approximation-based preprocessing. Moving on to two-dimensional signal processing, we described an additional algorithm for multiwavelet filtering (two rows at a time), and developed a new family of multiwavelets (the constrained pairs) that is well-suited to this two-row-at-a-time filtering.

We then applied this arsenal of techniques to two basic signal processing problems, denoising via thresholding (wavelet shrinkage), and data compression. After developing the approach via model problems in one dimension, we applied the various new multiwavelet approaches to the processing of images, frequently obtaining performance superior to the comparable scalar wavelet transform. These results suggest that further work in the design and application of multiwavelets to signal and image processing is well warranted.

Acknowledgments: We would like to thank Scott Hills for help programming the image compressions, and Stephane Mallat for useful discussions.

References

[1] B. Alpert, "A class of bases in L^2 for the sparse representation of integral operators," *SIAM J. Math. Analysis,* vol. 24, 1993.

[2] M. Antonini, M. Barlaud, P. Mathieu, and I. Daubechies, "Image coding using the wavelet transform," *IEEE Trans. on Image Processing,* vol. 1, pp. 205-220, 1992.

[3] R. H. Bamberger, S. L. Eddins, and V. Nuri, "Generalized symmetric extension for size-limited multirate filter banks," *IEEE Trans. on Image Proc.,* vol. 3, pp. 82-86, 1994.

[4] C. Brislawn, "Classification of symmetric wavelet transforms," Los Alamos Technical Report, 1993.

[5] B. V. Brower, "Low-bit-rate image compression evaluations," *Proc. SPIE*, Orlando, FL, April 4-9, 1994.

[6] I. Daubechies, *Ten Lectures on Wavelets*, Philadelphia: SIAM, 1992.

[7] D. Donoho, "De-noising by soft-thresholding," *IEEE Trans. Inf. Theory,* vol. 41, pp. 613-627, 1995.

[8] D. L. Donoho and I. M. Johnstone, "Ideal spatial adaptation via wavelet shrinkage," *Biometrika,* vol. 81, pp. 425-455, 1994.

[9] G. Donovan, J. Geronimo, and D. Hardin, "Intertwining multiresolution analyses and the construction of piecewise polynomial wavelets," preprint, 1994.

[10] Fed. Bureau of Investig., *WSQ Gray-Scale Fingerprint Image Compression Specification,* drafted by T. Hopper, C. Brislawn, and J. Bradley, IAFIS-IC-0110-v2, Feb. 1993.

[11] V. M. Gadre and R. K. Patney, "Vector multirate filtering and matrix filter banks," *Proc. IEEE ISCAS*, San Diego, 1992.

[12] J. Geronimo, D. Hardin, and P. R. Massopust, "Fractal functions and wavelet expansions based on several functions," *J. Approx. Theory,* vol. 78, pp. 373-401, 1994.

[13] R. A. Gopinath, J. E. Odegard, and C. S. Burrus, "Optimal wavelet representation of signals and the wavelet sampling theorem," *IEEE Trans. on Circ. and Sys. II,* vol. 41, pp. 262-277, 1994.

[14] C. Heil, G. Strang, and V. Strela, Approximation by translates of refinable functions," to appear in *Numerische Mathematik.*

[15] P. Heller, V. Strela, G. Strang, P. Topiwala, C. Heil, and L. Hills, "Multiwavelet filter banks for data compression," *Proc. IEEE ISCAS*, Seattle, WA, May 1995.

[16] H. Kiya, K. Nishikawa, and M. Iwahashi, "A Development of symmetric extension method for subband image coding," *IEEE Trans. on Image Proc.,* vol. 3, pp. 78-81, 1994.

[17] W. Lawton, S. L. Lee, and Z. Shen, "An algorithm for matrix extension and wavelet construction," *Mathematics of Computation,* to appear.

[18] S. Mallat, "A theory for multiresolution signal decomposition: the wavelet representation," *IEEE Trans. PAMI,* vol. 11, pp. 674-693, 1989.

[19] J. Odegard, M. Lang, H. Guo, R. Gopinath, and C. Burrus, "Nonlinear wavelet processing for enhancement of images," submitted to *IEEE SP Letters,* 1994.

[20] G. Plonka, "Approximation order of shift-invariant subspaces of $L^2(R)$ generated by refinable function vectors", preprint, 1995.

[21] G. Plonka, "Generalized spline wavelets", *Constr. Approx.*, to appear.

[22] J. M. Shapiro, "Embedded image coding using zerotrees of wavelet coefficients," *IEEE Trans. on SP,* vol. 41, pp. 3445-3662, 1993.

[23] Y. Shoham and A. Gersho, "Efficient bit allocation for an arbitrary set of quantizers," *IEEE Trans. ASSP*, vol. 36, pp. 1445-1453, 1988.

[24] M. J. T. Smith and S. Eddins, "Analysis-synthesis techniques for subband image coding," *IEEE Trans. ASSP,* vol. 38, pp. 1446-1456, 1990.

[25] G. Strang and T. Nguyen, *Wavelets and Filter Banks*, Wellesley, MA: Wellesley-Cambridge Press, 1995.

[26] G. Strang and V. Strela, "Short wavelets and matrix dilation equations," *IEEE Trans. on SP,* vol. 43, pp. 108-115, 1995.

[27] G. Strang and V. Strela, "Orthogonal multiwavelets with vanishing moments," *J. Optical Eng.,* vol. 33 , pp. 2104-2107, 1994.

[28] V. Strela and G. Strang, "Finite element multiwavelets," *Proc. NATO Conference, Maratea,* Boston, MA: Kluwer, 1995.

[29] G. Uytterhoeven, *Multiwavelets for image compression*, Masters thesis, Katholieke Universiteit Leuven, May, 1994.

[30] M. Vetterli and G. Strang, "Time-varying filter banks and multiwavelets," Sixth IEEE DSP Workshop, Yosemite, 1994.

[31] X.-G. Xia, J. Geronimo, D. Hardin, and B. Suter, "Computations of multiwavelet transforms", *Proc. SPIE 2569,* San Diego, CA, July 1995.

[32] W. Zettler, J. Huffman, and D. Linden. "The application of compactly supported wavelets to image compression," *Proc. SPIE* **1244**, pp. 150-160, 1990.